Uniosun Journal of Engineering and Environmental Sciences (UJEES), Vol. 7 No. 2, Sept. 2025
DOI: https//doi.org/10.64980/ujees.v7i2.449 **Enwerem et al.**
Published: September 30, 2025

THERMAL ANALYSIS OF FLY ASH REINFORCED AL-GR COMPOSITES

G. C. ENWEREM[1*], M. O. DUROWOJU[2], T. B. ASAFA[2], and P. A. OLUBAMBI[3]

[1]*Mechanical Engineering Department, Federal Polytechnic, Ede, Osun State, Nigeria.*
[2]*Mechanical Engineering Department, Ladoke Akintola University of Technology, Ogbomoso, Oyo State, Nigeria*
[3]*Centre for Nanoengineering and Advanced Materials (CeNAM), University of Johannesburg, South Africa*

[*]*Correspondent Author: chuks16a@gmail.com*

Abstract
Thermal dissipation and management are major problems of electronics and engineering materials that are exposed regularly to heat. Such materials warp or get distorted under thermal stresses due mainly to their material compositions. This work is aimed at studying the effects of reinforcement and thermal conditions on the thermal characteristics of fly ash reinforced Al-Gr composites produced through Conventional Sintering (CS) and Spark plasma sintering (SPS) methods. The Al-Gr matrix was reinforced with four different compositions of fly ash powder (0, 5, 10 and 15 wt.%). Composite samples were characterised through Scanning Electron Microscopy (SEM), Energy Dispersive Spectroscopy (EDS) and X-ray diffraction (XRD) for surface morphology, microstructure and phase composition. The composites were also comparatively subjected to Thermo-gravimetric Analysis (TGA), Differential Scanning Calorimetry (DSC), Differential Thermo-gravimetry (DTG), Thermal Conductivity (TC) and Coefficient of Thermal Expansion (CTE) analysis at 20 and 30 ^{o}C/min heating rates. The best thermal stability and conductivity were achieved at the heating rate of 30 ^{o}C/min, with the 15 wt.% Fly ash reinforcement using the SPS mode. The CTE showed a range of 1.813×10^{-5} to 1.89×10^{-5} /K for CS and 1.15×10^{-6} to 2.099×10^{-6} /K for SPS. Better thermal characteristics were achieved with fly ash reinforcement.

Keywords
Thermal Conductivity, Heating rates, Composite, Conventional Sintering, Fly ash, Reinforcement

1. INTRODUCTION

Global warming, driven by radical increases in temperature, has resulted in severe consequences ranging from human health hazards to thermal-induced failures in engineering systems and infrastructure (Shahzad, 2015; Abbass *et al.*, 2022; Hu *et al.*, 2023). Such thermal instabilities are of particular concern in applications operating under extreme thermal environments, including aerospace, automotive, and energy systems. In these sectors, the ability of materials to withstand, dissipate, and regulate heat is critical to maintaining safety, reliability, and performance. Consequently, extensive research efforts have been directed toward developing advanced thermal control systems capable of addressing heat acquisition, transport, and rejection while considering the demands of the operational environment (Scott *et al.*, 2010).

Effective thermal management systems require materials that combine reduced mass with the ability to sustain high heat fluxes while ensuring precise temperature control (Keltt and Bret, 2010). Currently, copper and aluminium are among the most widely employed materials in thermal management due to their favorable thermal conductivities (Wyszkowska, 2015). However, aluminium alloys suffer from severe limitations: they are prone to burning and degradation at elevated temperatures (Ceschini *et al.*, 2016; Saskarc, 2024). This constraint underscores the need for alternative or reinforced materials with higher melting points, superior thermal properties, and improved thermal stability.

Graphite, a crystalline allotrope of carbon, has emerged as a promising candidate owing to its low density (2.09–2.23 g/cm^3), high thermal conductivity (1500-2000 W/mK at room temperature), and layered hexagonal lattice structure. These properties make graphite attractive either as a reinforcement or as a potential replacement for aluminium in thermal management applications. However, its inherent brittleness and poor consolidation behavior present significant challenges during processing. Due to the weak Van der Waals bonding between adjacent graphene layers, graphite requires the presence of a wetting agent to

enhance surface interactions and promote bonding with metallic matrices. Previous studies have demonstrated that silica (SiO_2) serves as an effective wetting agent for graphite-based composites (Durowoju *et al.*, 2016).

An inexpensive and readily available source of SiO_2 is fly ash, an industrial by-product generated during coal combustion in power plants. Fly ash typically contains a high proportion of silica (up to ~51.43%) along with other oxides, making it an attractive option for use as a reinforcing and wetting agent in metal matrix composites (Rycroft, 2017). Beyond its technical benefits, the utilization of fly ash also presents environmental advantages by reducing industrial waste and promoting sustainable materials engineering.

In this study, the effects of varying fly ash content on the thermal properties of Al–Gr composites are investigated. Composites were fabricated using both spark plasma sintering (SPS), a rapid powder consolidation technique with superior densification, and conventional cold compaction followed by sintering. A comparative assessment is presented to evaluate how reinforcement composition and processing route influence the thermal performance of the resulting composites, with implications for advanced thermal management applications in aerospace, automotive, and energy industries.

2. MATERIALS AND METHOD

2.1 Initial powders and sample preparations

Graphite, fly ash and aluminium powder were used for this study. The graphite powder was obtained from the graphite rods in discarded dry cell batteries. The rods were extracted, washed, dried, and milled in a planetary ball milling machine (with tungsten carbide balls) at a speed of 200 rpm and a ball-to-powder ratio of 5:1 for 5 hours, to obtain a powdered particle size of 53 µm. Al powder (1-2 µm) was purchased from F.J. Broadmann & Co L.L.C, Haney, USA, while the fly ash powders were obtained as industrial wastes from Eskom Power Plant in South Africa, and sieved to a maximum particle size of 53 µm.

2.2 Composite formulation and fabrication

Graphite and aluminium powders were blended at a 1:4 ratio to serve as the matrix, which was subsequently reinforced with varying proportions of fly ash (Fla) powder (0, 5, 10, and 15 wt.%Fla). The powder mixtures were homogenised in a tubular mixer for 2 h to ensure uniform distribution of constituents and then employed for composite fabrication using two distinct techniques: Conventional Sintering (CS) and Spark Plasma Sintering (SPS). The CS samples were designated as CS0, CS5, CS10 and CS15, while the SPS samples had SP0, SP5, SP10 and SP15, based on the four sample compositions of 0, 5, 10, and 15 wt.%Fla. For the CS, the compaction was performed at room temperature using a 245 kN hydraulic press under an applied pressure of 305 MPa. The resulting green compacts were sintered in a muffle furnace at 500 °C, with a heating rate of 30 °C/min and a cooling rate of 10 °C/min to produce discs of 30 mm diameter. SPS processing was carried out using a High Heating Pressure Densification (HHPD25) unit under a uniaxial pressure of 50 MPa. The powders were sintered at 570 °C with a heating rate of 100 °C/min and a dwell time of 10 min, during which displacement was continuously monitored to assess the densification behaviour (Durowoju *et al.*, 2016).

2.3 Characterization

The powders and fabricated samples were characterized using X-ray Diffractometry (XRD), Scanning Electron Microscopy (SEM), Energy Dispersive Spectroscopy (EDS), Differential Scanning Calorimetry (DSC), Thermo-gravimetric Analysis (TGA), Differential Thermo-gravimetry (DTG), Thermal Conductivity (TC) and Coefficient of Thermal Expansion (CTE) analyses. XRD analysis was conducted using a Bruker D8 Advance diffractometer operated at 40 kV and 40 mA with Cu Kα radiation (λ = 0.15406 nm). The diffraction patterns were collected in the 2θ range of 20°–70° with a scan rate of 5°/min, and subsequently analyzed using X'Pert High Score Plus software. SEM investigations were performed using a JEOL JSM-7600F field emission microscope (Germany) with an accelerating voltage range of 0.1–30 kV, and elemental compositions were assessed via EDS.

Thermal analyses were carried out using a NETZSCH STA 449 F5 Jupiter system having a temperature range of −150–2400 °C. For each of DSC, TGA, and DTG analyses, approximately 5 mg of Al–Gr–Fla powder mixture was placed in a sample pan, while the reference pan was left empty. The samples were heated in a nitrogen atmosphere at a rate of 30 °C/min from 20 °C to 1000 °C to suppress oxidation. Thermal response curves were recorded in real time to provide insight into the phase transformations, mass changes, and decomposition behaviors of the samples. Thermal conductivity (k) values were estimated by applying Kissinger's method (Sah *et al.*, 2023), which relates DSC and TGA data to the thermal diffusivity (α) of the materials using equations (1) and (2).

$$k = \rho C_p \alpha \quad (1)$$

$$\alpha = \frac{\beta . \Delta T^2}{4.Tm^2} \quad (2)$$

Where ρ is the density (g/cm^3), C_p is the specific heat capacity (J/kgK), β is the heating rate (K/min), ΔT is the peak width (K), and T_m is the peak temperature (K). CTE was estimated using the modified Halpin-Tsai equation involving the rule of mixtures (Loos and Schulte, 2015).

3. RESULTS AND DISCUSSION

3.1 Microstructural analysis of the initial powders

The SEM-EDS micrographs of the starting powders are shown in Figure 1. The fly ash particles (Figure 1a) exhibited a predominantly spherical morphology with uniform size distribution and negligible agglomeration, consistent with observations reported in previous studies (Muruganandhan and Eswaramoorthi, 2014; Seetharaman *et al.*, 2022). In contrast, the aluminium particles (Figure 1c) displayed irregular morphologies, with some appearing flat or slightly curved. The graphite particles (Figure 1e) revealed a vermicular morphology, intermediate between nodular and flake shapes, and were characterized by a high carbon content.

Elemental analysis further confirmed these observations. The EDS spectrum of the fly ash powder (Figure 1b) revealed the presence of multiple elements, including Si, Ca, C, Mg, Fe, Al, Na, K, and O_2. The aluminium powder (Figure 1d) was composed predominantly of Al (98.2 wt.%), with a minor oxygen contribution (1.8 wt.%). The graphite powder (Figure 1f) exhibited a dominant carbon phase (93.1 wt.%), alongside minor amounts of oxygen (4.9 wt.%), calcium (0.1 wt.%), aluminium (1.5 wt.%), and silicon (0.3 wt.%). These trace elements are likely residual impurities introduced during the recovery of graphite rods from discarded dry cell batteries.

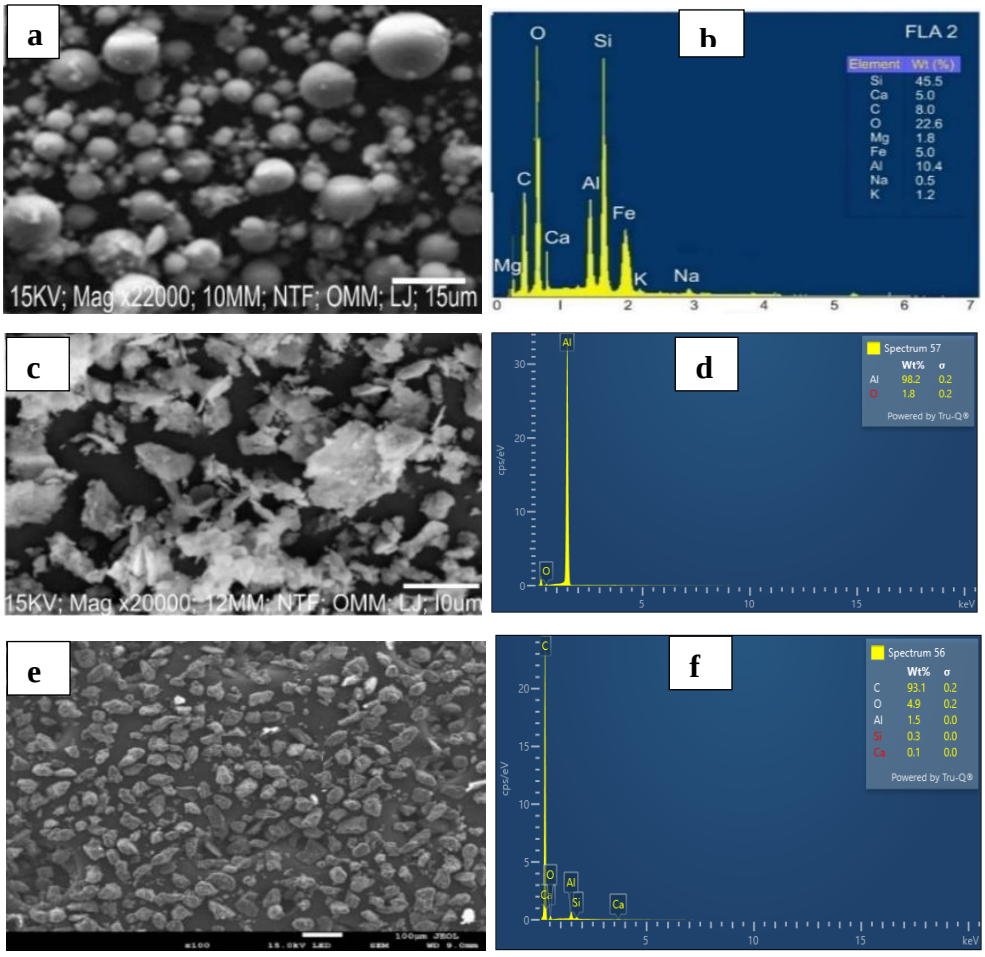

Figure 1: SEM-EDS micrograph for Fly ash powder (a and b), Aluminium powder (c and d) and Graphite powder (e and f).

3.2 Phase analysis of the fabricated samples

The XRD spectra for the samples fabricated by CS and SPS are presented in Figure 2. The presence of $CaCO_3$ and CaC_2 phases wa observed at the 5 wt.%tFla reinforcement of the CS samples (Figure 2a). These compounds are known to be hard abrasive materials. Due to the increase in fly ash content, the additional phases observed in the 10 wt.%Fla and 15 wt.%Fla reinforcements include MgO and TiO_2. The MgO was found to crystallise in a cubic structure, while the TiO_2 crystallised in an orthorhombic structure. The Al powder became oxidised into aluminium oxide (Al_2O_3). For sample SP5 (5 wt.%Fla), CaC_2, MgO, Al_2O_3 and SiO_2 phases were observed (Figure 2b). The Al_2O_3 and SiO_2 are ceramic in nature (Yu *et al.,* 2021; Zhang *et al.,* 2007), with very low coefficient of thermal expansion and good thermal shock resistance (Choktaweekam and Tangtermsirikul, 2009), while the CaC_2 is known to be reactive (Wang *et al.,* 2016). The increase in fly ash reinforcements showed increase in new phases like Ti, Fe_2Al, Fe_2O_3, TiO_2 as observed in the spectra of both CS and SPS samples, the effects of which will be felt in the areas of strength and thermal stability.

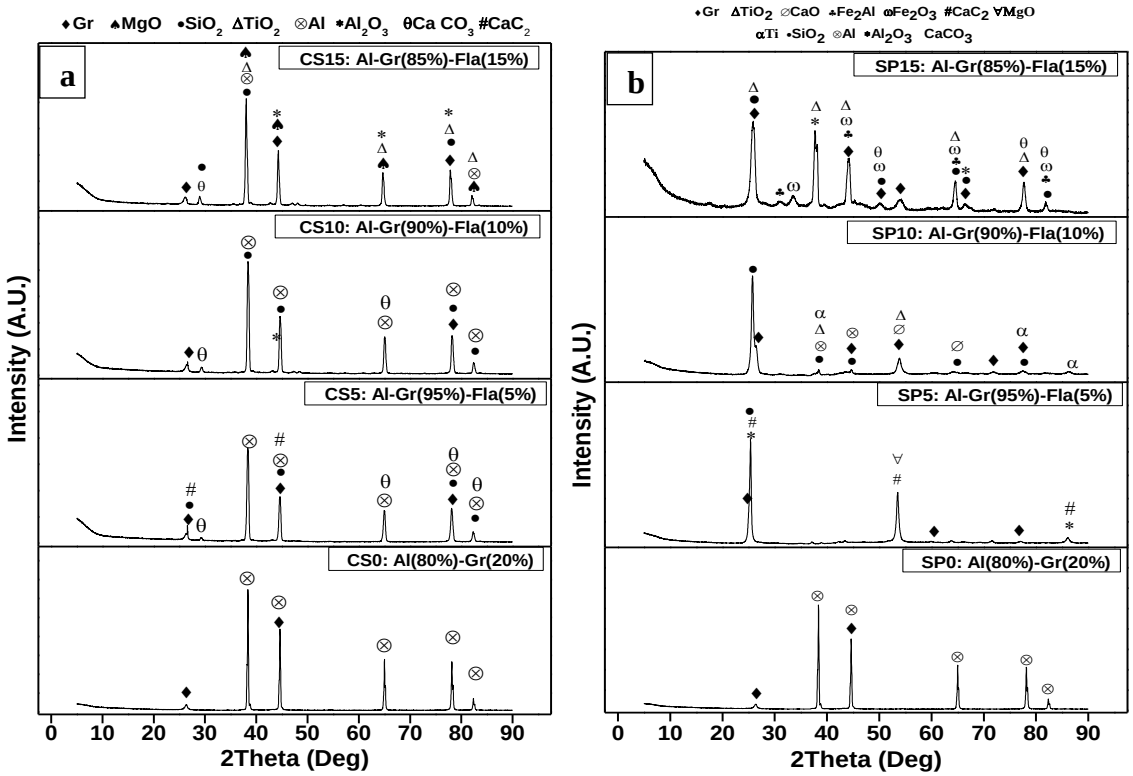

Figure 2: XRD patterns for the (a) four CS (denoted as CS0, CS5, CS10, and CS15) samples and the (b) four SPS samples (denoted as SP0, SP5, SP10, and SP15)

3.3 Effects of the change of heating rates on the TGA, DSC and DTG values of fly ash reinforced composites

The effects of fly ash variations on the TGA, DSC and DTG values (at a heating rate of 20 ^oC/min) of the fabricated samples when subjected to temperature gradients are presented in Figure 3. In the SPS samples, the highest weight loss was observed at 10 wt.%Fla, and at 15 wt.%Fla reinforcement for CS samples as shown in Figures 3 (a and b). At this same heating rate of 20 ^oC/min, the eight samples showed similar DSC thermal curves with the transition phases aligning around the temperature, 660 ^oC for both SPS and CS modes, as shown in Figures 3(c and d), which corresponds to the melting point of Aluminium (Ghanbari *et al.,* 2023). Three regions observable in the DTG curves as shown in Figure 3 (e and f) include desorption (involving moisture and volatile material weight losses), pyrolysis (involving possible molecular decompositions) and oxidation regions (Slopiecka *et al.,* 2012). These sections are indicated clearly in Figure 3f.

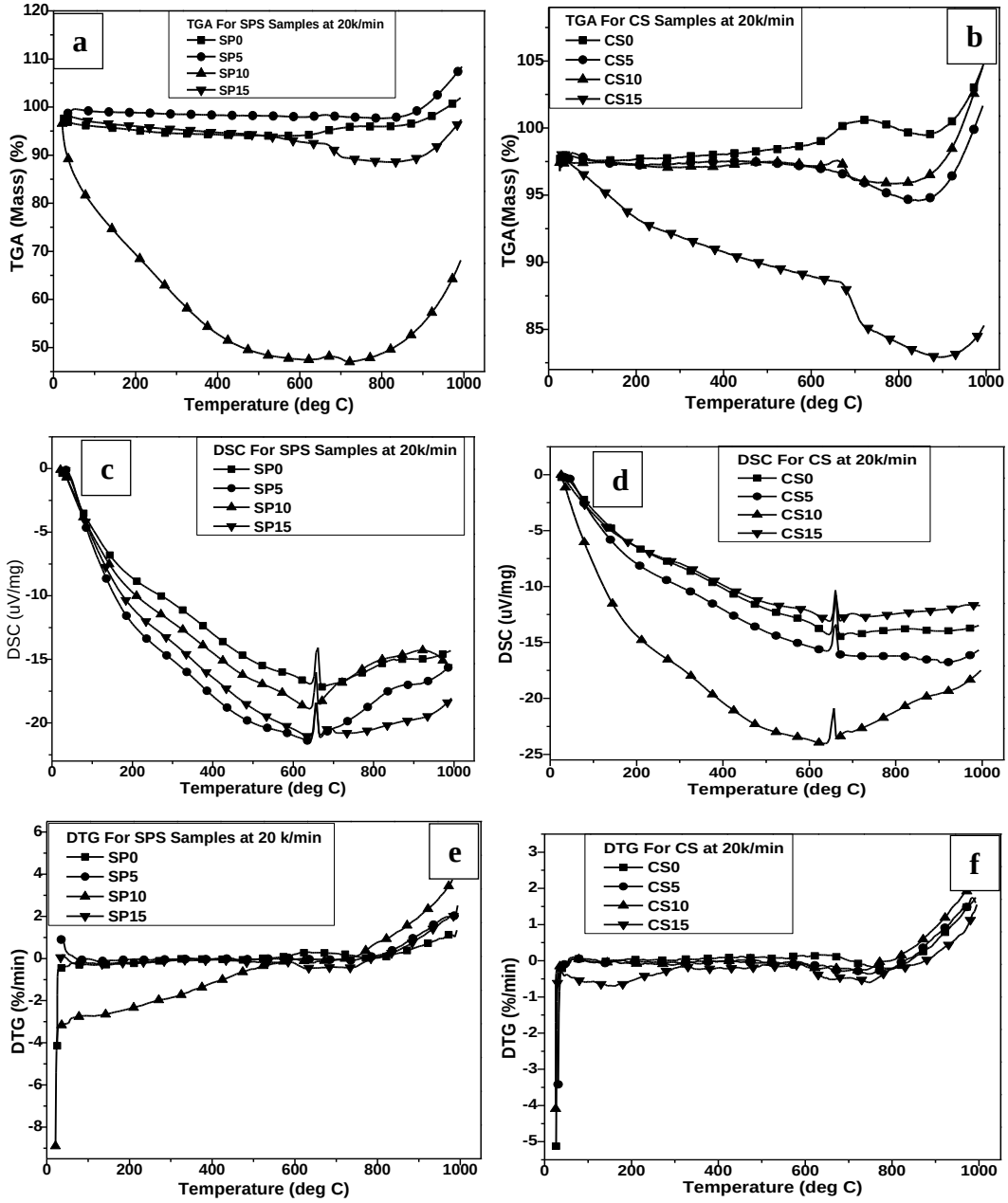

Figure 3: Comparative analysis of the effects of the fly ash content on the TGA (a and b), DSC (c and d) and DTG (e and f), at a heating rate of 20 ^{o}C/min, for the SPS and the CS samples respectively.

At the heating rate of 30 ^{o}C/min, comparative values of the TGA, DSC and DTG are presented in Figure 4 (a-f) for both SPS and C samples. In Figure 4 (a and b), the TGA results for CS and SPS samples are presented. The highest weight losses were recorded at 10 wt.%Fla and 15 wt.%Fla for the CS and SPS samples respectively. It could be observed that the best TGA stability was recorded at 5 wt.%Fla reinforcement for both CS and SPS samples. The DSC graphs (Figures 4c and 4d) showed similar thermal patterns for set of samples with each sample producing a peak around the 660 ^{o}C mark which corresponds to Al melting point. The DTG micrographs were partially aligned among the CS samples at 30 ^{o}C/min, while there was a noticeable gap between that of sample SP0 and SP15. This implies that an increase in the fly ash reinforcement affected the thermal decomposition of the composites. In all the 8 samples the rate of weight gain increased sharply from around 770 ^{o}C of heating. This DTG pattern may be connected to the identified MgO and TiO_2 phases in the XRD patterns of SP15 sample (Yang *et al.*, 2017; Kostova *et al.*, 2021).

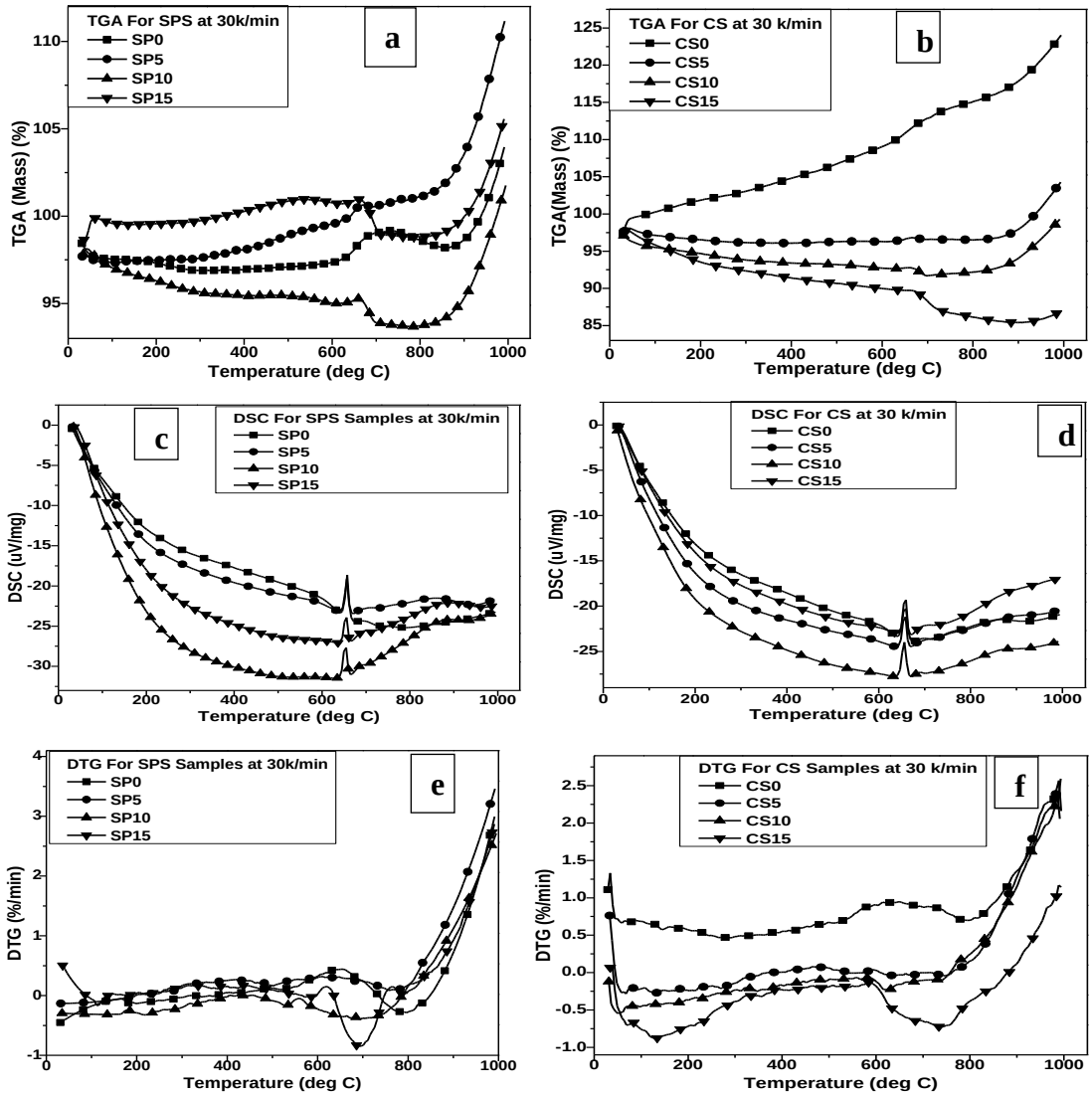

Figure 4: Comparative analysis of the effects of the fly ash content on the TGA (a and b), DSC (c and d) and DTG (e and f), at a heating rate of 30 ^{o}C/min, for the SPS and the CS samples, respectively.

Analysis of the weight loss or gain during the thermal tests is presented in Table 1. The highest average weight loss of 14.5% (equivalent to 0.725 g) after heating the samples to 1000 **^{o}C**, was observed at 10 wt.%Fla from the SPS fabrication method while the highest weight gain of 0.729 g (14.58%) was recorded at 0 wt.%Fla with the CS fabricated samples. The best thermal stability was observed at 15 wt.%Fla content. This indicates that the increase in fly ash reinforcement produced better thermal stability at elevated temperatures. The observed mass gains over some of the samples must have been the result of oxidation during the process, leading to the formation of oxides like alumina (Al_2O_3), silica (SiO_2), and Iron II oxide (Fe_2O_3) (Yu *et al.*, 2021; Kim *et al.*, 2023).

3.4 The effects of fly ash reinforcement and heating rates on the thermal conductivity (TC) and CTE values

The TC charts for all samples at the heating rates of 20 and 30 ^{o}C/min are shown in Figure 5a. At the 20 ^{o}C/min heating rate, the sample with 5 wt.%Fla produced the highest TC value of 3.368 W/mk among the 8 fabricated samples. This result is in line with existing research outcomes (Zhang *et al.*, 2019; Singh *et al.*, 2020; Wang *et al.*, 2020). The increase in fly ash reinforcement from 0 -15% produced approximately a 57.32 % reduction in TC among the CS samples and a 42.9% reduction in the TC of SPS-fabricated samples at 20 ^{o}C/min heating rate. There was a trend of reduction in TC value as the fly ash was increased. The declines in the TC values when fly ash contents were increased in the CS samples (at 30 ^{o}C/min heating rate) could be attributed to the low TC of fly ash particles and the none alignment of conductive particles of the matrix and reinforcement to produce percolation effects (Pietrak and Wisniewski, 2015). It could also mean

that the particles of fly ash reinforcement must have created interfaces and boundaries that disrupted the thermal transport pathway in the fabricated composite samples (Bigeralle and Lost, 2006).

Table 1: TGA residual weight loss or gain analysis of the fabricated samples. (The –ve signs indicate weight loss, while +ve signs represent weight gain)

Sample ID	Residual weight loss/gain at 20 ^{o}C/min. (%)	Residual Temp at 20 ^{o}C/min (^{o}C)	Residual weight loss/gain at 30 ^{o}C/min. (%)	Residual Temp at 30 ^{o}C/min (^{o}C)	Average weight loss/gain (%)
CS0	5.00	671.92	24.15	674.31	+14.58
CS5	2.10	901.77	4.47	638.07	+3.29
CS10	5.08	636.98	-0.40	636.11	+2.34
CS15	-14.61	645.03	-12.94	669.03	-13.78
SP0	2.20	671.85	4.40	786.37	+3.30
SP5	8.25	640.37	11.49	672.28	+9.87
SP10	-30.80	642.06	1.81	629.78	-14.50
SP15	-2.24	638.80	5.97	636.03	+1.87

However, there was an inconsistent increase in TC for the SPS samples which could be attributed to non-uniform distribution of fly ash reinforcement causing possibly varying interfacial bonding between the matrix and the fly ash particles.

There was a resulting pattern of consistent increase in the CTE value with increasing wt.%Fla among the CS samples (Figure 5b), but among the SPS samples, there was an inconsistent reduction in CTE as the fly ash is increased (Figure 5c). Samples SP10 and SP15 showed 36.06 % and 46.5 % reductions in CTE over the control sample respectively.

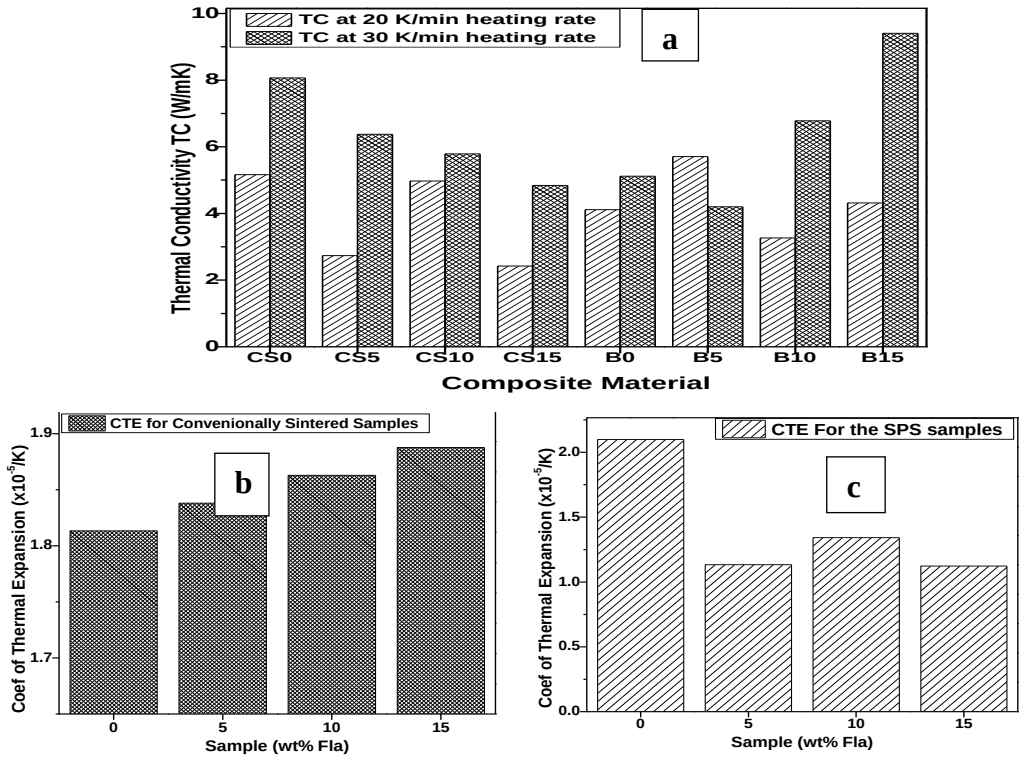

Figure 5: Thermal charts showing (a) the TC for the CS and the SPS samples at 20 ^{o}C/min and 30 ^{o}C/min heating rates, (b) the CTE for the CS samples and (c) the CTE for the SPS samples at the different fly ash compositions.

4. CONCLUSION

The thermal analysis revealed that increasing fly ash content generally reduced the average weight loss for conventionally sintered samples. The melting point of aluminium was observed around 660 °C for all samples. Thermal conductivity decreased with increasing fly ash content for conventionally sintered samples at both heating rates. For SPS samples, the trend was less consistent. SP15 (15 wt.%Fla) exhibited the highest thermal conductivity at 30°C/min. SPS samples showed decreases in coefficient of thermal expansion (CTE) with increasing fly ash, while conventionally sintered samples exhibited the opposite trend.

REFERENCES

[1] Shahzad, U.R. "Global Warming: Causes, Effects and Solutions", *Durreesamin Journal*.. https://www.researchgate.net/publication/316691239. 1(4), 2015. ISSN: 2204-9827

[2] Abbass, K., Qasim, M.Z., and Song, H. "A review of the global climate change impacts, adaptation, and sustainable mitigation measures", *Environmental Science Pollution Research*. . https://doi.org/10.1007/s11356-022-19718-6. **29**, 2022. pp 42539–42559.

[3] Hu, D., Grilli, N., Yan, W. (2023). ''Dislocation structures formation induced by thermal stress in additive manufacturing: Multiscale crystal plasticity modeling of dislocation transport'', *Journal of the Mechanics and Physics of Solids*.. https://doi.org/10.1016/j.jmps.2023.105235. 173, 2023, 105235.

[4] Scott, A.H, Christopher, K., Brain, M., William, N., Steven, R., and Theodore, S., ''Draft Thermal Management Systems Roadmap Technology Area 14'', *National Aeronautics and Space Administration*, 2010, TA14.1- TA14-30.

[5] Klett, J., and Bret, C., *Thermal management solutions utilizing high thermal conductivity graphite foams*, Oak Ridge National library. https://www.researchgate.net/publication/266269710. 2010, pp 1-11.

[6] Wyszkowska, E., ''Research and Development of Advanced Aluminium/graphite Composites for Thermal Management Applications'' Unpublished M. Sc. Dissertation, University of Science and Technology Geneve, Department of Foundry Engineering, Geneve, 2015, pp 1-99.

[7] Ceschini, L., Morri, A., Balducci, E., Cavina, N., Rojo, N., Calogero, L., Poggio, L., ''Experimental observations of engine piston damage induced by knocking combustion'' Elsevier. *Materials and Design*. https://doi:10.1016/j.matdes.2016.11.015. 2016, S0264127516314022. Article in press.

[8] Saskarc Inc. Group Company, ''Metal alloys for fabrication: Understanding the strength and weaknesses in metal alloys for fabrication'', www.saskarc.com. Accessed on December 15, 2024.

[9] Durowoju, M. O., Sadiku, E. R., Diouf, S., Shongwe, M. B., Olubambi, P. A., Mekgwe, N., and Ramakokovhu, ''Effect of micron and nano-sized ZrB_2 addition on the Microstructure and properties of Spark Plasma Sintered Graphite-Aluminium hybrid Composite'', *Journal of Material Science: Materials in Electronics*. https://DOI.10.1007/s10854-016-4346-3. 27(5), 2016, pp 4672-4688

[10] Rycroft, M., *Exploring the many uses of Fly-ash*, EE Publishers, www.ee.co.za. 2017.

[11] Sah, P.K., Kumar, S.S., and Sreedeep, S., ''Thermal conductivity and specific volume heat capacity of bentonite–fly ash-based fluidized thermal backfill'', *Journal of Thermal Analysis and Calorimetry*. https://doi.org/10.1007/s10973-023-12523-4. 148, 2023, pp 11607–11617.

[12] Loos, M.R., and Schulte, K., *Is It Worth the Effort to Reinforce Polymers with Carbon Nanotubes? Carbon Nanotube Reinforced Composites*, PDL Handbook series. https://doi.org/10.1016/C2012-0-06123-6. 2015, ISBN:978-1-4557-3195-4.

[13] Muruganandhan, P., and Eswaramoorthi, M., ''Aluminium Composite with Fly Ash – A Review'', *IOSR Journal of Mechanical and Civil Engineering*, 11(6), Ver III, 2014, pp 38-41.

[14] Seetharaman, S., Subramanian, J., Singh, R.A., Wong, W.L.E., Nai, M.L.S., and Gupta, M., ''Mechanical properties of Sustainable Metal matrix composites: A review on the role of Green reinforcements and processing methods'' *Technologies*. https://doi.org/10.3390/technologies10010032. 10(32), 2022, pp 1-27.

[15] Yu, Q., Yong, D., Yuebin, F., and Ziyong, L., ''Phase Transformation of Alumina, Silica and Iron Oxide during Carbothermic Reduction of Fly Ash for Ceramics Production'', *Metals*. https://doi.org/10.3390/met11081165. 11(8), 2021, pp 1165-1170.

[16] Zhang, F.C., Luo, H.H., and Roberts, S.G., ''Mechanical properties and microstructure of Al_2O_3/mullite composite'' *Journal Material Science*. https://doi.org/10.1007/s10853-006-1402-z. 42, 2007, pp 6798-6802.

[17] Choktaweekarn, P., and Tangtermsirikul, S., ''A model for predicting the coefficient of thermal expansion of cementitious paste'', *Science Asia*. https://doi:10.2306/scienceasia1513-1874.2009.35.057. 35, 2009, pp 57–63.

[18] Wang, L., Huang, X., Li, D., Huang, Y., Bao, K., Li, F., Wu, G., Liu, B., and Cui, T., ''Pressure-induced structural transformation of CaC_2'', *The Journal of Chemical Physics*. https://doi:10.1063/1.4948705. 144(19), 2016, p194506.

[19] Ghanbari, E., Stephen, J.P., Jan, H.V.E., ''Analysis of differential scanning calorimetry (DSC): determining the transition temperatures, and enthalpy and heat capacity changes in multicomponent systems by analytical model fitting'', *Journal of Thermal Analysis and Calorimetry*. https://doi.org/10.1007/s10973-023-12356-1. 148, 2023, pp 12393–12409.

[20] Slopiecka, K., Bartocci, P., and Fantozzi, F., ''Thermogravimetric analysis and kinetic study of poplar wood pyrolysis'', *Applied Energy*, 97, 2012, pp 491-497.

[21] Yang, K., Qiu, X., Qu, F., Zeng, X., and Wang, P., ''Application of XRD and TG-DTG-DTA for Analysis of Content and Components of Asphalt in CA Mortar'', *Journal of Building Materials*. https://Doi:10.3969/j.issn.1007-9629.2017.05.027. 20, 2017, pp 820-826.

[22] Kostova, B., Petkova, V., Kostov-Kytin, V., Tzvetanova, Y., Avdeev, G., ''TG/DTG-DSC and high temperature in-situ XRD analysis of natural thaumasite'', *Thermochimica Acta*, 697, 2021, 178863.

[23] Kim, Y., Choi, S., Kim, Y., Kang, C., Hong, S., ''Changes in thermal properties of 7075 aluminium alloy by aging heat treatment'', *Materials Science and Technology*. https://doi:10.1080/02670836.2022.2163745. 39(10), 2023, pp 1208-1213.

[24] Zhang, Y., Liu, H., and Wang, X., ''Graphite-aluminium composites for thermal management'', Composites Part A: *Applied Science and Manufacturing*, 121, 2019, pp 241-248.

[25] Singh, R., Singh, S., and Singh, R., ''Thermal conductivity of graphite-aluminium composites'', *Journal of Composite Materials*, 54(11), 2020, pp1523-1534.

[26] Wang, X., Liu, H., and Zhang, Y., ''Graphite-aluminium composites for thermal management'', *Composites Part A: Applied Science and Manufacturing*, 135, 2020, p105924.

[27] Pietrak, K, and Wisniewski, T.S., ''A review of models for effective thermal conductivity of composite materials'', *Journal of Power Technologies*. 95(1), 2015, pp 14–24.

[28] Bigeralle, M., and Lost, A., ''Perimeter analysis of Von Koch Island, Application to the evolution of grain boundaries during heating'', *Journal of Material Science*, 41, 2006, pp 2509-2516.